

Parent (half)metal and emergent superconductivity in rhombohedral trilayer graphene

András L. Szabó¹ and Bitan Roy^{2,*}

¹Max-Planck-Institut für Physik komplexer Systeme, Nöthnitzer Str. 38, 01187 Dresden, Germany

²Department of Physics, Lehigh University, Bethlehem, Pennsylvania, 18015, USA

(Dated: September 5, 2022)

Combining mean-field and renormalization group analyses, here we shed light on recently observed superconductivity and their parent states in chemically doped rhombohedral trilayer graphene, subject to external electric displacement fields [1]. We argue that close to the charge neutrality, on site Hubbard repulsion favors layer antiferromagnet, which when combined with the displacement field (inducing layer polarization), produces a spin-polarized, but valley or isospin unpolarized half-metal, conducive to the nucleation of spin-triplet f -wave pairing (SC2). By contrast, at larger doping Kekulé valence bond order emerges as a prominent candidate for isospin coherent paramagnet, boosting condensation of spin-singlet Cooper pairs in the conventional s -wave channel (SC1), manifesting a “selection rule” among competing orders. Responses of these paired states to displacement and in-plane magnetic fields show qualitative similarities with experimental observation.

Introduction. Carbon based atom-thick layers of honeycomb membrane open up a rich landscape harboring peculiar band dispersion of gapless chiral quasiparticles, when stacked in the out-of-plane direction [2, 3]. As such, Bernal bilayer graphene and rhombohedral trilayer graphene (RTLG) respectively accommodate bi-quadratic [4] and bi-cubic [5] band touchings at two independent corners of the hexagonal Brillouin zone, giving rise to SU(2) valley or isospin degrees of freedom. Twist by a relatively small, so-called magic angle ($\sim 1^\circ$) between two honeycomb layers produces nearly flat bands of slow massless Dirac fermions [6–10], where superconductivity has been observed and studied extensively in experiments over the last few years [11–14]. More recently, superconductivity in structurally simpler RTLG has been reported, when it is chemically doped and subject to external electric displacement field (D) in the stacking direction [1]. Culmination of these recent experimental achievements places us at the dawn of the carbon age of superconductivity. The present work is geared toward unfolding the nature of the superconducting orders and their adjacent parent (half)metallic states in RTLG.

We begin by reviewing the key experimental observations and summarizing our main results related to superconductivity and their parent correlated metallic states in RTLG. Near the charge neutrality, doped RTLG supports a spin-polarized but valley unpolarized *half-metal*, in the presence of D -fields, as suggested by quantum oscillation measurements. It is expected that Hubbard repulsion dominates in graphene-based layered materials at least near charge neutrality [15]. It favors layer antiferromagnet with a staggered pattern of electronic spins between two low energy sites, residing on the top and bottom layers. By contrast, the D -field induces layer polarization of electronic density. Either of these two orders leads to a uniform and isotropic gap in the quasiparticle spectra. But electronic bands loose two-fold spin degeneracy near each valley when they are present simultaneously, producing a spin-polarized, valley unpolarized half-metal

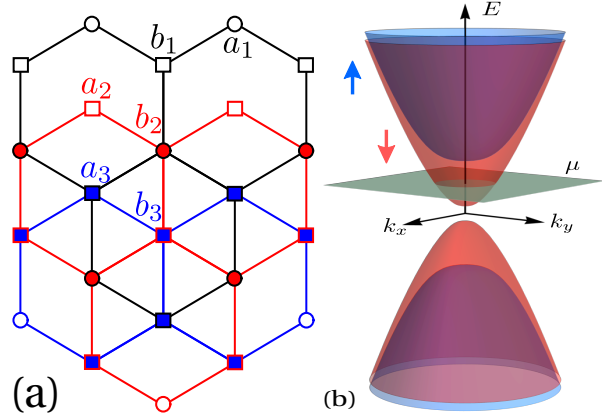


FIG. 1. (a) Top view of rhombohedral trilayer graphene (RTLG), with the subscript denoting the layer index $i = 1, 2, 3$ of the sites. Each a_1 and b_2 sites, as well as each a_2 and a_3 sites overlap. The eigenstates of the high energy split-off bands reside dominantly on these four overlapping dimer sites, while b_1 and a_3 sites participate in the low-energy description of RTLG, featuring bi-cubic band touchings [Eq. (1)]. (b) A spin polarized half-metal resulting from the combination of Hubbard repulsion driven layer antiferromagnet and external electric displacement field induced layer polarization. The frozen spin orientation of the half-metal is, however, arbitrary.

[Fig. 1]. Such Hubbard repulsion driven antiferromagnetic insulator, giving away to a half-metal in the presence of D -fields has also been reported in Ref. [16].

The half-metal by virtue of being spin polarized sustains only spin-triplet pairing between electrons with equal spin projection. There are *four* competing local triplet pairings in RTLG. With the assistance of the D -field an f -wave pairing [Fig. 2(b)] becomes energetically favored [Fig. 3(a)]. The Cooper pairs in this state are formed by electrons with equal spin projection that reside on the same layer and the superconducting wave-function changes sign six times under 2π rotation in the real space and Brillouin zone [Fig. 2(b)]. The f -wave pairing fully

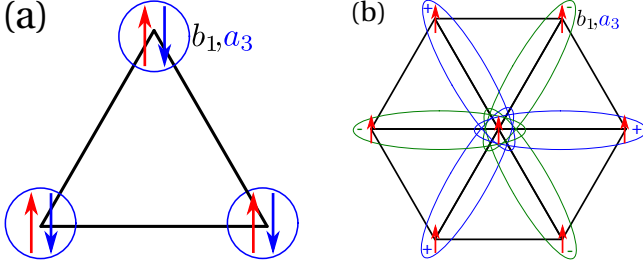


FIG. 2. Schematic representations of Cooper pairs for (a) spin-singlet *s*-wave and (b) spin-triplet *f*-wave pairings, formed within the sites belonging to the same layer (top or bottom) of RTLG. The *s*-wave (*f*-wave) pairing is the candidate for the pairing order SC1 (SC2) [1].

and isotropically gap the entire Fermi surface of the half-metal. The resulting phase diagram in the (μ, u) plane shows qualitative agreement with experiments [Fig. 3(b)]. Here μ is the chemical doping measured from the cubic band touching point and u is the voltage bias between the top and bottom layers, yielding $D = -u/(2d_0)$, where d_0 is the interlayer separation. This triplet paired state is named SC2 in Ref. [1], and it naturally exceeds the Pauli limiting in-plane magnetic field.

As the system is tuned further away from the charge neutrality, another superconducting state (SC1) appears, stemming from a valley or isospin coherent parent paramagnetic metal. In RTLG there are three candidates for such metallic state, among which the one featuring Kekulé pattern of hopping between the low energy sites living on the top and bottom layers is always energetically advantageous [Fig. 4(a)]. The Kekulé valence bond order (KVBO) breaks the translational symmetry and receives additional boost from the D -field. Thus the isospin coherent paramagnetic metal manifests KVBO.

When repulsive electron-electron interaction in the KVBO channel dominates in RTLG, besides supporting the KVBO order itself, it is also conducive for the condensation of electrons into Cooper pairs in the conventional spin-singlet *s*-wave channel [Fig. 4(b)]. We arrive at this conclusion from a renormalization group (RG) calculation. Appearance of the *s*-wave pairing as the representative of SC1 is qualitatively consistent with the observed Pauli limiting in-plane magnetic field [1]. Additionally, the fact that weaker D -field favors such an *s*-wave superconductor is also in qualitative agreement with our findings [Fig. 4(c)]. Nucleation of the *s*-wave pairing follows a recently proposed “selection rule” among competing orders [17–19], as it constitutes a composite $O(5)$ supervector of competing masses for cubic quasiparticles in RTLG with KVBO and externally induced layer polarization.

Model. We arrive at these key results by considering the low-energy description for electronic bands in RTLG [20–22]. The unit cell is composed of six sites, each layer contributing to two of them [Fig. 1(a)]. But, one set of site

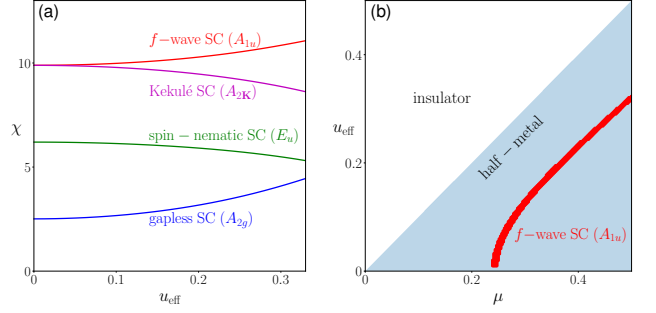


FIG. 3. (a) Bare mean field susceptibility χ [Eq. (2)] of four spin-triplet pairings in a spin polarized half-metal as a function of the effective interlayer potential difference $u_{\text{eff}} = |u - \Delta_{\text{LAF}}|$ for chemical doping $\mu = 0.5$ and temperature $t = 0.05$, promoting the *f*-wave pairing with largest susceptibility as the most prominent candidate for SC2. Here $\chi, \mu, t, u_{\text{eff}}$ are dimensionless and measured in appropriate units of α [Eq. (1)]. (b) The line of constant susceptibility ($\chi = 20$) for the *f*-wave pairing in the (μ, u_{eff}) plane qualitatively agrees with experimentally observed line of superconductivity in the (n_e, D) plane, where n_e is the carrier density.

from the bottom (a_1) and top (b_3) layers reside on top of both set of sites (b_2 and a_2 , respectively) of the middle layer (dimer-sites). While the intralayer nearest-neighbor hopping (t_0) gives rise to massless Dirac fermions, the direct hopping (t_{\perp}) between the dimer-sites pushes four out of six bands to high-energies ($\sim t_{\perp} \approx 200$ meV), the split-off bands, leaving only two bands near the charge neutrality point displaying cubic band touchings. Wavefunctions of the cubic bands predominantly live on the b_1 and a_3 sites near two inequivalent valleys at the corners of the hexagonal Brillouin zone. Accounting for the layer or equivalently sublattice, valley and spin degrees of freedom, we arrive at the single-particle Hamiltonian for noninteracting electrons in RTLG

$$H_0 = \alpha [f_1(\mathbf{k})\Gamma_{3031} + f_2(\mathbf{k})\Gamma_{3002}] + u\Gamma_{3003} - \mu\Gamma_{3000}, \quad (1)$$

where $\alpha = t_0^3 a^3 / t_{\perp}$, $f_1(\mathbf{k}) = k_x(k_x^2 - 3k_y^2)$ and $f_2(\mathbf{k}) = -k_y(k_y^2 - 3k_x^2)$, a is the lattice spacing, and momentum \mathbf{k} is measured from respective valleys. Electron (hole) doping corresponds to $\mu > 0$ ($\mu < 0$). The sixteen-dimensional Hermitian matrices are $\Gamma_{\mu\nu\rho\lambda} = \eta_{\mu}\sigma_{\nu}\tau_{\rho}\beta_{\lambda}$, where $\{\eta_{\mu}\}$, $\{\sigma_{\nu}\}$, $\{\tau_{\rho}\}$ and $\{\beta_{\lambda}\}$ are four sets of Pauli matrices respectively operating on the Nambu or particle-hole, spin, valley or isospin and layer or sublattice indices, with $\mu, \nu, \rho, \lambda = 0, \dots, 3$. We Nambu double the theory to facilitate the forthcoming discussion on superconductivity. It is worth mentioning that the dimer hopping t_{\perp} couples quasirelativistic Dirac fermions on honeycomb flatland as a static non-Abelian magnetic field [23]. Thus the resulting chiral cubic quasiparticles are representatives of planar non-Abelian fermions.

Here we neglect particle-hole asymmetry and trigonal warping. The latter splits the momentum space vortex

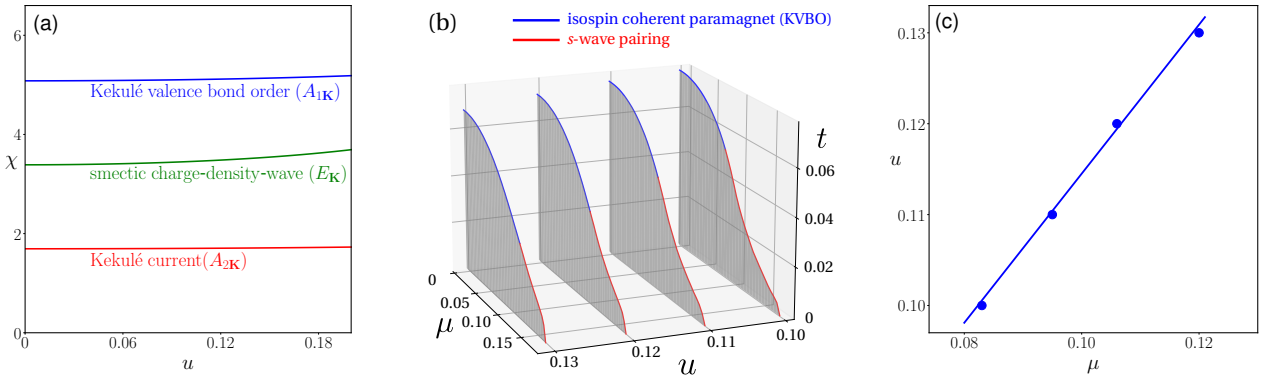


FIG. 4. (a) Bare mean field susceptibility (χ) of three isospin coherent paramagnetic orders as a function of u (interlayer voltage bias) for $\mu = 0.5$ and $t = 0.05$, promoting the KVBO with the largest susceptibility as the most prominent candidate. (b) Various cuts of the phase diagram for a fixed bare interaction strength $\lambda_{A_{1K}} = 0.2$ showing a competition between KVBO and s -wave pairing. The shaded (white) region represents ordered (disordered) phase. (c) Onset points for the s -wave pairing in the (μ, u) plane obtained from (b), showing qualitative similarities with experimental observation. For larger μ (u) the order phase is s -wave pairing (paramagnetic metal with KVBO). Here all the parameters are dimensionless (see text).

of vorticities ± 3 near two valleys for cubic quasiparticles into three Dirac points with vorticities ± 1 , preserving the overall topology of the band touching points. As the density of states for cubic (Dirac) fermions diverges (vanishes) as $\varrho(E) \sim |E|^{-1/3}$ ($\varrho(E) \sim |E|$), strong correlation effects are driven by cubic chiral fermions.

Half-metal and superconductivity. In graphene based systems, onsite Hubbard repulsion is the dominant component of finite-range Coulomb interactions [15] that near half filling favors layer antiferromagnet on an effective bipartite lattice for RTLG in terms of the low energy sites b_1 and a_3 [Fig. 1(a)]. It leads to a staggered pattern of electronic spin between them, and when acquires a finite amplitude Δ_{LAF} it is accompanied by the matrix Γ_{0303} . Here without any loss of generality we choose the spin quantization axis in the z direction. The resulting two-fold valley degenerate quasiparticle spectra are given by

$$\pm \sqrt{\alpha^2 |\mathbf{k}|^6 + (u \pm \Delta_{\text{LAF}})^2} - \mu$$

that lack the spin degeneracy. When $|u - \Delta_{\text{LAF}}| < \mu < u + \Delta_{\text{LAF}}$, we realize a spin polarized, but valley unpolarized half-metal, since both layer antiferromagnet and layer polarization are insensitive to the valley degrees of freedom (appearing with the identity τ_0 matrix in the valley space). The effective single-particle Hamiltonian (H_0^{HM}) describing the half metal takes the form of H_0 [Eq. (1)], with $u \rightarrow u_{\text{eff}} = |u - \Delta_{\text{LAF}}| < \mu$ and without the spin degrees of freedom, as the system behaves like an effective spinless one with frozen spin orientation.

The superconductor resulting from the half-metal is constrained to be a spin-triplet, with Cooper pairs forming between electrons with equal spin projection. RTLG altogether supports four spin-triplet superconductors: an f -wave pairing (A_{1u}), a Kekulé pair-density-wave (A_{2K}), a spin nematic pairing (E_u) and a gapless pairing (A_{2g}).

Their irreducible representations under D_{3d} point group are shown in the parentheses. The pairing matrices are

$$\Gamma_{\mu 30}, (\Gamma_{\mu 12}, \Gamma_{\mu 22}), (\Gamma_{\mu 31}, \Gamma_{\mu 02}), \text{ and } \Gamma_{\mu 33}, \text{ respectively.}$$

Here $\Gamma_{\mu \rho \lambda} = \eta_{\mu} \tau_{\rho} \beta_{\lambda}$, and $\mu = 1, 2$ reflects the $U(1)$ gauge redundancy of the superconducting phase. Only Kekulé and spin nematic pairings transform as doublets.

To access and compare the propensities toward the formation of triplet paired states in a half-metal, we compute their bare mean field susceptibility, given by

$$\chi = -T \sum_{n=-\infty}^{\infty} \int \frac{d^2 \mathbf{k}}{(2\pi)^2} \text{Tr} [G(i\omega_n, \mathbf{k}) M G(i\omega_n, \mathbf{k}) M] \quad (2)$$

for zero external frequency and momentum, when the paired state is represented by the matrix M . The fermionic Green's function $G(i\omega_n, \mathbf{k}) = [i\omega_n - H_0^{\text{HM}}]^{-1}$, $\omega_n = (2n + 1)\pi T$ are the fermionic Matsubara frequencies, T is the temperature, and the Boltzmann constant $k_B = 1$. The results are shown in Fig. 3. As the f -wave [24] and translational symmetry breaking Kekulé [25] pairings are superconducting masses, they possess largest degenerate susceptibility for zero D -field.

External D -field lifts this degeneracy, as the f -wave (Kekulé) pairing anticommutes (commutes) with $\Gamma_{303} = \eta_3 \tau_0 \beta_3$, the matrix accompanying the displacement field in the half-metal manifold. In general, the D -field increases the propensity toward nucleation of any paired state that anticommutes with Γ_{303} . Nonetheless, the f -wave pairing continues to acquire largest susceptibility for any finite μ and u_{eff} . It thus stands as the most promising candidate for the observed triplet pairing emerging from a spin polarized half-metal, namely SC2.

As $D \propto u$ or u_{eff} and carrier density $n_e \sim \mu$, we can scrutinize the effect of the displacement field and carrier density on SC2 from the dependence of χ on μ and u_{eff} . Notice that $\chi \propto T_c$ (transition temperature) and Δ (amplitude) of the paired state. Hence, a line of constant χ in the (μ, u_{eff}) plane should qualitatively mimic the observed line of superconductivity in the (n_e, D) plane. With increasing D -field the degree of layer polarization increases pushing the system closer to insulation. Therefore, to compensate this propensity toward field induced insulation, a larger carrier density or chemical doping is required to observe superconductivity in RLG, as found in experiments and also in our obtained scaling of the constant χ line in the (μ, u_{eff}) plane [Fig. 3(b)].

Paramagnetic metal and superconductivity. We now proceed to larger doping regime, where the system supports a valley or isospin coherent paramagnetic metal, bordering a superconductor (SC1) [1]. Isospin coherence implies that two valleys get coupled, thereby resulting in translational symmetry breaking. The translational symmetry in graphenelike systems in the low-energy continuum limit translates into a U(1) symmetry, generated by $\Gamma_{0030} = \eta_0 \sigma_0 \tau_3 \beta_0$ [19, 26]. The paramagnetic nature of the metallic state indicates that it is spin-singlet. Then there are three candidates for such a state: KVBO ($A_{1\mathbf{K}}$), Kekulé current ($A_{2\mathbf{K}}$) and smectic charge-density-wave ($E_{\mathbf{K}}$). The corresponding irreducible representations of D_{3d} point group is shown inside the parentheses. These orders are accompanied by the matrices

$\Gamma_{30\rho 1}, \Gamma_{00\rho 2}$, and $(\Gamma_{30\rho 0}, \Gamma_{30\rho 3})$, respectively.

Here $\rho = 1, 2$ manifests the U(1) valley coherence. The smectic charge-density-wave also breaks the rotational symmetry about the z direction by an angle $\pi/2$, generated by Γ_{0033} . We compute and compare the susceptibilities of these three orders at finite doping and interlayer voltage bias (u), defined in Eq. (2) with $G(i\omega_n, \mathbf{k}) = [i\omega_n - H_0]^{-1}$ and H_0 given in Eq. (1). The results are shown in Fig. 4(a). The KVBO possesses the largest susceptibility and is thus the most prominent candidate for the isospin coherent paramagnetic metal. This is so because the KVBO is a mass for cubic quasiparticles and the associated matrices ($\Gamma_{3011}, \Gamma_{3021}$) also anticommute with the one appearing with the voltage bias (Γ_{3003}).

To shed light on the nature of the pairing, originating from such a correlated metal, we perform a leading-order RG analysis by considering a four-fermion interaction

$$g_{A_{1\mathbf{K}}} \left[(\Psi^\dagger \Gamma_{3011} \Psi)^2 + (\Psi^\dagger \Gamma_{3021} \Psi)^2 \right]$$

that favors KVBO. Sixteen-component Nambu-doubled spinors Ψ^\dagger and Ψ involve spin, valley and layer or sublattice (b_1 and a_3) degrees of freedom. Besides demonstrating the stability of KVBO, we showcase the emergence of superconductivity at low temperatures and finite chemical doping from a pure *repulsive* interaction $g_{A_{1\mathbf{K}}} > 0$,

following the Kohn-Luttinger mechanism [27, 28]. We integrate out the fast Fourier modes residing within a thin Wilsonian momentum shell with $\Lambda e^{-\ell} < |\mathbf{k}| < \Lambda$. Here Λ is the ultraviolet momentum cutoff up to which the quasiparticle spectra remain cubic with momentum and ℓ is the logarithm of the coarse grain scale. The coupled differential RG flow equations read

$$\frac{d\lambda_{A_{1\mathbf{K}}}}{d\ell} = \lambda_{A_{1\mathbf{K}}} + \lambda_{A_{1\mathbf{K}}}^2 H(t, \mu, u) \quad \text{and} \quad \frac{dx}{d\ell} = 3x, \quad (3)$$

for $x = t, \mu, u$. The dimensionless quantities are defined as $\lambda_{A_{1\mathbf{K}}} = g_{A_{1\mathbf{K}}} / (\alpha \Lambda 8\pi)$, $t = T / (\alpha \Lambda^3)$, $\tilde{\mu} = \mu / (\alpha \Lambda^3)$ and $\tilde{u} = u / (\alpha \Lambda^3)$. For brevity we take $\tilde{\mu} \rightarrow \mu$ and $\tilde{u} \rightarrow u$. The flow equation of x gives an infrared cut-off $\ell_x^* = \ln[x^{-1}(0)]/3$ for $x = t, \mu$ and u , where $x(0) < 1$ corresponds to its bare value. The function $H(t, \mu, u)$ is quite lengthy and not particularly informative. Even though the four-fermion coupling $\lambda_{A_{1\mathbf{K}}}$ is a *relevant* parameter due to the divergent density of states of cubic fermions, its RG flow terminates at $\ell^* = \min(\ell_t^*, \ell_\mu^*, \ell_u^*)$. Then the system describes an ordered (a disordered) phase when $\lambda_{A_{1\mathbf{K}}}(\ell^*) > 1 (< 1)$.

Only KVBO and spin-singlet *s*-wave pairing can be realized in the ordered phase. To capture their competition, we simultaneously allow the conjugate fields, coupling with the corresponding fermion bilinears as

$$\Delta_{A_{1\mathbf{K}}} \sum_{\rho=1,2} \Psi^\dagger \Gamma_{30\rho 1} \Psi \quad \text{and} \quad \Delta_{A_{1g}} \sum_{\mu=1,2} \Psi^\dagger \Gamma_{\mu 000} \Psi,$$

respectively, to flow under coarse grain. The RG flow equations for the conjugate fields are given by

$$\frac{d \ln \Delta_y}{d\ell} - 3 = \lambda_{A_{1\mathbf{K}}} I_y(t, \mu, u), \quad \text{for } y = A_{1\mathbf{K}} \text{ and } A_{1g}. \quad (4)$$

The I functions are also quite lengthy and not particularly informative. As $\lambda_{A_{1\mathbf{K}}}$ diverges, indicating onset of an ordered phase, the pattern of symmetry breaking is determined by the conjugate field that diverges toward $+\infty$ fastest. Following this prescription we construct few cuts of the phase diagram in the (μ, t) plane for a fixed bare $\lambda_{A_{1\mathbf{K}}}$ and for various values of u [Fig. 4(b)].

At sufficiently low (high) temperatures the ordered phase supports an *s*-wave pairing (a paramagnetic metal with KVBO), manifesting an “organizing principle” based on a generalized energy-entropy argument [18, 19]. The *s*-wave superconductor isotropically gaps the entire Fermi surface and is thus energetically favored at low temperature. By contrast, KVBO metal occupies the high-temperature regime, as it carries more entropy due to the presence of gapless quasiparticles. The paired state solely stems from quantum fluctuations of incipient KVBO in a metal without any long range order. With increasing u or D -field as the system appears at the shore of insulation, a larger chemical doping is required to induce superconductivity [Fig. 4(c)], similar to the situation for

SC2 and as also observed in experiments. In the presence of electronic interaction in the KVBO channel, the appearance of the *s*-wave pairing as SC1 follows a “selection rule” [17–19], since the matrices involving the paired state, KVBO and *D*-field induced layer polarization

$$\{\Gamma_{1000}, \Gamma_{2000}, \Gamma_{3011}, \Gamma_{3021}, \Gamma_{3003}\}$$

constitute a unique O(5) composite vector of competing masses for cubic chiral fermions.

Discussions. Guided by the phenomenology of a recent experiment [1], here we identify the prominent candidates of (half)metallic phases and the resulting proximal superconductors. KVBO in a paramagnetic metal should feature new diffraction peaks due to broken translational symmetry. The nature of the paired states can be pinned from tunneling spectroscopy (gapped or gapless) and Josephson junction (pairing symmetry). Our discussion should therefore stimulate future experiments, underpinning the symmetries of these correlated phases. The present theoretical framework will be extended to study the nature of correlated quarter-metal in RLG [29], and possible proximal superconductivity in the future.

Acknowledgments. B.R. was supported by a Startup grant from Lehigh University. We thank Andrea F. Young for useful correspondence.

Note added. After completing this work, we became aware of few preprints, also discussing competing phases and superconductivity in RLG [30–32].

* Corresponding author: bitan.roy@lehigh.edu

- [1] H. Zhou, T. Xie, T. Taniguchi, K. Watanabe, A. F. Young, arXiv:2106.07640
- [2] M. I. Katsnelson, *Graphene: Carbon in Two Dimensions* (Cambridge University Press, Cambridge, U.K., 2012).
- [3] A. H. Castro Neto, F. Guinea, N. M. R. Peres, K. S. Novoselov, and A. K. Geim, Rev. Mod. Phys. **81**, 109 (2009).
- [4] K. S. Novoselov, E. McCann, S. V. Morozov, V. I. Falko, M. I. Katsnelson, U. Zeitler, D. Jiang, F. Schedin, and A. K. Geim, Nat. Phys. **2**, 177 (2006).
- [5] L. Zhang, Y. Zhang, J. Camacho, M. Khodas, and I. Zaliznyak, Nat. Phys. **7**, 953 (2011).
- [6] J. M. B. L. dos Santos, N. M. R. Peres, and A. H. Castro Neto, Phys. Rev. Lett. **99**, 256802 (2007)
- [7] R. Bistritzer and A. H. MacDonald, Proc. Natl. Acad. Sci. USA **108**, 12233 (2011).
- [8] B. Roy and K. Yang, Phys. Rev. B **88**, 241107(R) (2013).
- [9] H.-C. Po, L. Zou, A. Vishwanath, and T. Senthil, Phys. Rev. X **8**, 031089 (2018).
- [10] B. A. Bernevig, Z.-D. Song, N. Regnault, and B. Lian, Phys. Rev. B **103**, 205411 (2021).
- [11] Y. Cao, V. Fatemi, S. Fang, K. Watanabe, T. Taniguchi, E. Kaxiras, and P. Jarillo-Herrero, Nature (London) **556**, 43 (2018).
- [12] X. Lu, P. Stepanov, W. Yang, M. Xie, M. A. Aamir, I. Das, C. Urgell, K. Watanabe, T. Taniguchi, G. Zhang, A. Bachtold, A. H. MacDonald, and D. K. Efetov, Nature **574**, 653 (2019).
- [13] M. Yankowitz, S. Chen, H. Polshyn, K. Watanabe, T. Taniguchi, D. Graf, A. F. Young, C. R. Dean, Science **363**, 1059 (2019).
- [14] U. Zondiner, A. Rozen, D. Rodan-Legrain, Y. Cao, R. Queiroz, T. Taniguchi, K. Watanabe, Y. Oreg, F. von Oppen, A. Stern, E. Berg, P. Jarillo-Herrero, and S. Ilani, Nature (London) **582**, 203 (2020).
- [15] T. O. Wehling, E. Şaşioğlu, C. Friedrich, A. I. Lichtenstein, M. I. Katsnelson, and S. Blügel, Phys. Rev. Lett. **106**, 236805 (2011).
- [16] Y. Lee, S. Che, J. Velasco Jr., D. Tran, J. Baima, F. Mauri, M. Calandra, M. Bockrath, C. N. Lau, arXiv:1911.04450
- [17] B. Roy and V. Jurićć, Phys. Rev. B **99**, 121407(R) (2019).
- [18] A. L. Szabó, R. Moessner and B. Roy, Phys. Rev. B **103**, 165139 (2021).
- [19] A. L. Szabó and B. Roy, Phys. Rev. B **103**, 205135 (2021).
- [20] M. Koshino and E. McCann, Phys. Rev. B **80**, 165409 (2009).
- [21] F. Zhang, B. Sahu, H. Min, and A. H. MacDonald, Phys. Rev. B **82**, 035409 (2010).
- [22] V. Cvetkovic and O. Vafek, arXiv:1210.4923
- [23] R. M. A. Dantas, F. Peña-Benitez, B. Roy, and P. Surówka, Phys. Rev. Research **2**, 013007 (2020).
- [24] C. Honerkamp, Phys. Rev. Lett. **100**, 146404 (2008).
- [25] B. Roy and I. F. Herbut, Phys. Rev. B **82**, 035429 (2010).
- [26] I. F. Herbut, V. Jurićć and B. Roy, **79**, 085116 (2009).
- [27] W. Kohn and J. M. Luttinger, Phys. Rev. Lett. **15**, 524 (1965).
- [28] M. A. Baranov, A. V. Chubukov, and M. Yu. Kagan, Int. J. Mod. Phys. B **06**, 2471 (1992).
- [29] H. Zhou, T. Xie, A. Ghazaryan, T. Holder, J. R. Ehrets, E. M. Spanton, T. Taniguchi, K. Watanabe, E. Berg, M. Serbyn, A. F. Young, arXiv:2104.00653
- [30] S. Chatterjee, T. Wang, E. Berg, and M. P. Zaletel, arXiv:2109.00002
- [31] A. Ghazaryan, T. Holder, M. Serbyn, and E. Berg, arXiv:2109.00011
- [32] Z. Dong and L. Levitov, arXiv:2109.01133